ORIGINAL PAPER

Determination of the electrochemically active surface area by CO and hydrogen of PtSnRuTa/C-based electrocatalysts and their relationship with catalytic activity against alcohol oxidation

Maria Aparecida Ribeiro Queiroz[1] · Maria de Lourdes Soprani Vasconcellos[1] · Marcos Antônio Ribeiro[1] · Priscila Paiva Luz[1] · Felipe de Moura Souza[2,3] · Mauro Coelho dos Santos[2] · Marco C. C. Guimarães[4] · José Ricardo Cezar Salgado[5] · Rolando Pedicini[6] · Josimar Ribeiro[1]

Abstract

This work studies the influence of the addition of tantalum to the ternary PtSnRu/C electrocatalysts on the oxidation of different alcohols: methanol, ethanol, ethylene glycol, and glycerol. The physical–chemical characterizations showed an increase in the lattice parameter of the fcc (face-centered cubic) structure of Pt due to the incorporation of Sn and/or Ta metals that evidence of alloy formation. The nanoparticles range from 3.8 to 9.8 nm and present a homogeneous distribution on carbon. CO stripping voltammetry measurements were used to obtain the electrochemically active surface area (ECSA) of electrocatalysts, which showed higher values for the quaternary electrocatalysts of composition $Pt_{24.8}Sn_{5.0}Ru_{1.0}Ta_{7.7}/C$ (21.3 m^2 g$_{Pt}^{-1}$), $Pt_{8.1}Sn_{1.3}Ru_{1.2}Ta_{1.0}/C$ (29.3 m^2 g$_{Pt}^{-1}$), and $Pt_{8.9}Sn_{1.0}Ru_{1.5}Ta_{1.5}/C$ (39.4 m^2 g$_{Pt}^{-1}$). The $Pt_{8.9}Sn_{1.0}Ru_{1.5}Ta_{1.5}/C$ electrocatalyst presented high peak currents, compared with the other electrocatalysts, using cyclic voltammetry for methanol, ethanol, ethylene glycol, and glycerol. In chronoamperometry on ethanol, ethylene glycol, and glycerol, the $Pt_{8.9}Sn_{1.0}Ru_{1.5}Ta_{1.5}/C$ electrocatalyst showed higher currents (24, 18, and 19 A g$_{Pt}^{-1}$, respectively) compared to the other electrocatalysts. The results showed that the addition of Ru and Ta on PtSn/C nanoparticles led to an increase in the ECSA values. It can be suggested that the presence of the quaternary electrocatalyst maximizes the electronic and bifunctional mechanism which are responsible to increase the electrocatalytic activity to the alcohol oxidation. In addition, the presence of Ru and Ta together with Sn on Pt/C nanoparticles was also related to increased stability, representing an alternative for use in direct alcohol fuel cells.

Keywords Electrocatalyst · Platinum · Tantalum · Electrochemically active surface area · Direct alcohol fuel cells

✉ Josimar Ribeiro
josimar.ribeiro@ufes.br

1 Laboratório de Pesquisa E Desenvolvimento Em Eletroquímica (LPDE), Departamento de Química, Centro de Ciências Exatas, Universidade Federal Do Espírito Santo, Campus Goiabeiras, Av. Fernando Ferrari, Vitória, ES 29075-910, Brazil

2 Laboratório de Eletroquímica E Materiais Nanoestruturados (LEMN) - Centro de Ciências Naturais E Humanas (CCNH), Universidade Federal Do ABC (UFABC), CEP, Rua Santa Adélia 166, Bairro Bangu, Santo André, SP 09210-170, Brazil

3 Instituto Federal Goiano, CEP, Rodovia BR153, KM633 Zona Rural , Morrinhos, GO 75650-000, Brazil

4 Departamento de Morfologia, Centro de Ciências da Saúde, Universidade Federal Do Espírito Santo, Campus Maruípe, Vitória, ES 29049-999, Brazil

5 Instituto Latino Americano de Ciências da Vida E da Natureza, Universidade Federal da Integração Latino-Americana, Foz do Iguaçu, PR 85866-900, Brazil

6 Instituto Di Tecnologia Avanzate Per L'Energia "Nicola Giordano" (ITAE) - Via S. Lucia Sopra Contesse, 5-98126 Messina, Italy

Introduction

Fuel cells are devices that convert chemical energy into electrical energy from electrons there are in chemical bonds (dos Santos et al. 2017a, b; Ong et al. 2017). Polymer electrolyte fuel cells (PEFC) and direct alcohol fuel cells (DAFC) have higher efficiency than internal combustion engines because they are working at low temperatures (Pedicini et al. 2014; Wu 2016). Fuel storage is a problem in PEFC systems. Given that the hydrogen is currently stored in gas or liquid, causing energy expenditure and issues related to the safety of high-pressure systems (Pedicini et al. 2014; Moura Souza et al. 2018). For this reason, DAFC systems show significant advantages because alcohol storage is effortless, without energy expenditure and risks of explosions (Soloveichik 2014; Badwal et al. 2015). Additionally, DAFCs is simpler, as the fuel feeds the cell directly to the anode without the need for any chemical modification or removal of impurities (Pedicini et al. 2014; Wu 2016).

The alcohols used in such fuel cells are generally methanol, ethanol, ethylene glycol, and glycerol because they are in the liquid phase under ambient conditions, relatively simple, and easy to store and transport (Soloveichik 2014; dos Santos et al. 2017a, b; Souza et al. 2020). As methanol has easy electrooxidation, it has been widely studied as fuel for DAFC (Cohen et al. 2007; Puthiyapura et al. 2018; Lu et al. 2020). However, because it had a high crossover rate, methanol presented less efficiency than expected, decreasing the efficiency of the cell. Another associated problem is its toxicity, which must be handled attention (Cohen et al. 2007; Ong et al. 2017; Puthiyapura et al. 2018; Lu et al. 2020).

Ethanol has some advantages over methanol, as it is nontoxic, a lower crossover rate, and it can be obtained from renewable sources. However, the complete electrooxidation of ethanol is hampered and leads to a loss of efficiency compared to methanol due a C–C bond (Fujiwara et al. 2008; Ong et al. 2017). Ethylene glycol is widely used as an automotive antifreeze and the presence of an additional hydroxyl, compared to ethanol, causes a lower vapor pressure, reducing evaporation losses (Neto et al. 2005; Pan et al. 2019).

Glycerol is an oily, water-soluble, odorless, nonflammable, and nontoxic liquid (Huber et al. 2006; Maya-Cornejo et al. 2016). In the biodiesel production, glycerol is obtained as a by-product, reaching 10% in the production chain (Basha et al. 2009). As a by-product in biodiesel production, glycerol has a low cost and a high theoretical energy density (6400 Wh L^{-1}), making it a good alternative as a fuel for DAFC (Maya-Cornejo et al. 2016; Ong et al. 2017).

Low-temperature fuel cells like DAFCs need materials with high the electrocatalytic activity, such as Pt, to perform well at temperatures below 100 °C (Breeze 2019; Li & Baek 2020). However, the need to use Pt-based electrocatalysts significantly increases the cost of production due to limited reserves left (Shao-Horn et al. 2007; Saleh and Easton 2014). In this context, metals such as Sn and Ru are widely used to obtain electrocatalysts with electrocatalytic activity and stability superior to Pt (Liu et al. 2011; Zheng et al. 2011). They can increase electrocatalytic activity due to the geometric effect and the bifunctional mechanism (Dimakis et al. 2009; Kim et al. 2011). Furthermore, in the bifunctional mechanism, auxiliary metals Sn and Ru can produce oxygenated species that facilitate the oxidation and desorption of the intermediate strongly adsorbed on Pt sites (Queiroz and Ribeiro 2019). Therefore, the use of ternary electrocatalysts with PtSnRu composition for the electrooxidation of small organic molecules has been studied frequently due to the pointed benefits (Zhang et al. 2021). Notwithstanding, low tolerance to CO is still a challenge to be overcome in alcohol electrooxidation reactions (Rizo et al. 2017).

Alternatively, the presence of tantalum on Pt-based electrocatalysts leads to having improved tolerance to carbon monoxide (CO), leading to increased oxidation and indicating a synergistic effect between metals on Pt electrocatalysts (Ueda et al. 2003; Awaludin et al. 2011). Queiroz and Ribeiro (2019) reported a study of the composition of PtSnRuTa/C quaternary electrocatalysts for direct ethanol fuel cell (DEFC) where the addition of Ta modified the crystalline structure of Pt, decreasing the adsorption strength of the intermediates and increasing the oxygenated species by bifunctional mechanism. According to the study, the best composition for DEFC was the following $Pt_7Sn_1Ta_1Ru_1$ molar ratio.

Besides, Zhao et al. (2019) reported a Pd/Ta_2O_5-Pt electrocatalyst that exhibits excellent catalytic activity toward the electrooxidation of ethylene glycol (EG) in acid conditions. A finding is the increase in conductivity in the ternary composition of the electrocatalyst. Furthermore, Zhao et al. (Xin and Shen 2017) reported a study using the La-Ta_2O_5/Pt electrocatalyst for glycerol oxidation reaction (GOR). They indicated that modification with Ta_2O_5 in electrocatalysts increased GOR kinetics than Au- and Pt-based electrocatalysts.

There are also studies in which Pt-based electrocatalysts modified with Ta in which the electrooxidation of methanol (Masud et al. 2012), formaldehyde (Masud et al. 2011a, b), formic acid (Masud et al. 2011a, b), and ethanol (Queiroz and Ribeiro 2019) was investigated. These studies found that the presence of Ta increased electrocatalytic activity due to the bifunctional mechanism and the electronic effect (Gregoire et al. 2010; Queiroz and Ribeiro 2019). Studies associate the increased electrocatalytic activity of electrocatalysts due to a less positive potential for H_2O oxidation for

OH species compared to pure Pt catalysts (Kakinuma et al. 2017). In this way, the catalytic sites of Pt are free so that the oxidation reaction can continue more quickly. However, no more specific study to compare the contribution of Ta- and Pt-based electrocatalysts in small alcohols is yet available.

We report a complete composition study of PtSnRuTa/C quaternary electrocatalysts with the comparison of methanol, ethanol, ethylene glycol, and glycerol as fuel oxidation to fill a gap in the real possibilities of these alcohols to DAFC technologies. Additionally, we investigate the CO stripping in these electrocatalysts to know whether the electrocatalysts are better at decreasing CO poisoning at different surfaces.

Experimental section

Preparation of electrocatalysts

Two ternary PtSnRu/C and PtSnTa/C (7:1:2% mol) electrocatalysts were synthesized with molar ratios (Pt:Sn:Ru or Ta) and three quaternary PtSnRuTa/C electrocatalysts with different molar ratios, 7:1:1:1; 14:2:1:3; and 14:2:3:1 (% mol). The polymeric precursors' method was used, where 40% is metal and 60% is carbon black (Vulcan XC72 carbon support (Cabot) treated with HNO_3 1.0 mol L^{-1} with 70% purity) (Ribeiro et al. 2007, 2008; Artem et al. 2012; Teran et al. 2012; Santos et al. 2017a, b; El Attar et al. 2020). Initially, resins of the metal precursors were prepared separately using a mixture of citric acid (99% purity Sigma-Aldrich) and ethylene glycol (99.8% purity Sigma-Aldrich), in the molar ratio of 1:4:16 to metal, citric acid, and ethylene glycol, respectively. This mixture was heated around 65 °C in heating plate (DiagTech DT3110H) until the complete citric acid dissolution. A solution of the metal ions in isopropanol (99.9% purity NEON), with a concentration of 0.05 mol L^{-1}, was added dropwise, maintaining a constant temperature. After this step, the polymerization stage was carried out by heating the system under stirring in a temperature range between 80 and 95 °C, and subsequently, the evaporation of excess ethanol was performed. The exact values of the metallic resin concentrations were determined by gravimetry measurements, obtaining the following values: 1.51×10^{-4} mol of Pt g^{-1}; 7.34×10^{-5} mol of Sn g^{-1}; 1.23×10^{-4} mol of Ta g^{-1}; and 1.57×10^{-4} mol of Ru g^{-1}. The synthesis of the electrocatalysts followed these steps: 40 mg carbon was mixed with the metallic-organic resins in 5-mL glass bottles with 1.0 mL of ethanol (96% purity Sigma-Aldrich), to facilitate the dispersion of all materials. The obtained mixture was homogenized in an ultrasonic bath (UNIQUE USC-1400) for 30 min. Thermal treatment in the oven at 60 °C for 24 h was performed (QUIMIS Q317M-22) to remove the residual solvent. The electrocatalysts were obtained after calcination at 350 °C in an oven (QUIMIS Q318M) for 30 min under an air atmosphere. The calcination temperature was chosen according to the thermogravimetric analysis data (see Figure S1 in supplementary material). All precursor solutions were prepared using ultrapure water (SARTORIUS mini, Arium®, Göttingen, Germany) with a resistivity of 18.2 MΩ cm at 22 ± 2 °C.

Physical characterization

The X-ray diffraction patterns were obtained using a diffractometer (Bruker D8) with Cu Kα radiation (1.5406 Å) and 2θ scanning from 10 to 90° (0.01° min^{-1}). The crystallite size was estimated using Scherrer Eq. (1) (Moura Souza et al. 2018) for all diffraction planes:

$$D = \frac{K\lambda}{\beta cos\theta_\beta} \tag{1}$$

D corresponds to the apparent size of the crystallite, K to the form factor (0.9 for spherical crystallite), λ the radiation wavelength (1.5406 Å), β peak width at half-height of the maximum intensity, and θ_β the angle corresponding to the maximum peak intensity. The cell parameters for each material were obtained by applying Bragg's Eq. (2) fitted using the least-square procedure with a pseudo-Voigt curve to obtain the values of diffraction angles. The final value of cell parameters is the average value calculated from each reflection fit. For the cubic system, the following expression can be used (Moura Souza et al. 2018).

$$d_{hkl} = \frac{a^2}{h^2 + k^2 + l^2} \tag{2}$$

Scanning Electron Microscope Carl Zeiss (EVO10) was used; moreover, quantitative analysis for each sample was carried out using an X-ray dispersive energy spectroscopy detector (EDS) coupled with an SEM apparatus.

A more in-depth study has been conducted by Transmission Electron Microscopy (TEM)—Electron Microscope Model JEOL (JEM-1400), with 800 k magnification and 120 kV voltage.

Electrochemical measurements

Electrochemical experiments were performed with an electrochemical cell of 50 mL with three electrodes: Ag/AgCl reference electrode (ANALION, R682A) with saturated KCl solution, a graphite electrode with an area of 3.15 cm^2 as the counter electrode (CE), and a glassy carbon working electrode with an area of 0.046 cm^2 (ANALION, K5705).

Before each electrochemical measurement, a cleaning treatment on the surface of the glassy carbon working electrode was performed using a 0.3-μm alumina suspension

(SKILL-TEC) on suede paper with the help of the metallo-graphic sander Aropol VV (arotec), washed with ultrapure water, and dried at room temperature for 30 min. After drying, 20 µL of ink of electrocatalytic material was added to the polished surface of the glassy carbon working electrode. The ink of the electrocatalytic material was prepared using 1.0 mg of one of the electrocatalyst compositions with 5 µL of Nafion® (Sigma-Aldrich) and 95 µL ethanol (Sigma-Aldrich), which were added in a 1.5-mL microcentrifuge tube and taken to the USC-1400 ultrasonic bath (UNIQUE) for 30 min, forming a homogeneous ink.

Measurements of cyclic voltammetry, chronoamperometry, and chronopotentiometry were taken in a PAR-Ametek Potentiostat/Galvanostat VersaSTAT4, at an ambient temperature of 22 ± 2 °C. Before each measurement, to remove the oxygen dissolved in the solution of the system, a nitrogen purging gas was used for 15 min.

Cyclic voltammetry (CV) was used to evaluate the electrocatalytic activity of materials synthesized in H_2SO_4 0.5 mol L^{-1} and in the presence of alcohols such as methanol, ethanol, ethylene glycol, and glycerol with a concentration of 1.0 mol L^{-1}. For all cyclic voltammetry measurements, the potential range from −0.15 to 1.2 V versus Ag/AgCl and scan rate of 20 mV s^{-1} was used.

To evaluate the oxidation profile of carbon monoxide for electrocatalysts, a CO stripping voltammetry was performed. The potential at 0.1 V versus Ag/AgCl was applied to the working electrode for 40 min where the first 20 min CO was bubbled into the solution to saturate it, and afterward, the last 20 min, N_2 was bubbled to remove excess CO in the solution. Finally, two consecutive cyclic voltammograms were obtained with a potential scanning range from −0.15 to 1.2 V versus Ag/AgCl. Electrochemically active surface area (ECSA) was calculated having the reference charge for the oxidation of a carbon monoxide or hydrogen monolayer on a platinum electrode corresponding to 420 µC cm^{-2} for CO and 210 µC cm^{-2} for hydrogen, as shown in Eqs. 3 and 4 (Binninger et al. 2014; Łukaszewski 2016). A correction for double-layer charging by subtracting the charge density between 0.10 and 0.60 V versus Ag/AgCl from CV curves was considered.

$$ESCA_{CO}(m^2 g_{Pt}^{-1}) = \frac{Q_{CO}}{420 \times wt_{Pt}} \quad (3)$$

$$ESCA_H(m^2 g_{Pt}^{-1}) = \frac{Q_H}{210 \times wt_{Pt}} \quad (4)$$

Q_{CO} is the charge density of carbon monoxide, Q_H is the charge density of hydrogen monolayer, and wt_{Pt} is the amount of platinum dispersed in the volume of the electrocatalytic material deposited on the surface of the working electrode (Łukaszewski 2016).

To assess the stability of the voltammetric profile of the electrocatalysts, a total of 1000 cycles were performed with a scan rate of 50 mV s^{-1} between −0.15 and 1.2 V versus Ag/AgCl. To measure the stability of the electrocatalysts, ECSA was obtained after 50, 500, and 1000 cycles using both the hydrogen desorption and CO oxidation charge anodic.

Chronoamperometry measurements were taken in methanol, ethanol, ethylene glycol, and glycerol with a concentration of 1.0 mol L^{-1} in H_2SO_4 0.5 mol L^{-1}, applying a potential of 0.4 V versus Ag/AgCl for 7200 s, and chronopotentiometry applying a current density of 3 mA cm^{-2} for 15 h.

Results and discussion

Physical characterization

Figure 1 shows the X-ray diffraction patterns of the electrocatalysts. All the electrocatalysts showed diffraction peaks referring to the diffraction planes (111), (200), (220), (311), and (222) of the platinum pattern with a face-centered cubic structure (fcc) and spatial group Fm-3 m (JCPDS 04-802) (Queiroz & Ribeiro 2019). As shown in Fig. 1, all electrocatalysts showed a preferential orientation of the crystallographic planes at (111), presenting the highest intensities among the diffraction peaks presented. Characteristic peaks associated with metals or even metallic oxides of Sn, Ru, and Ta were not observed. However, the presence of these metals and even their oxides in small amounts should not be ruled out, as XRD shows signs of crystalline particles and not amorphous particles, thus suggesting the formation of a solid solution.
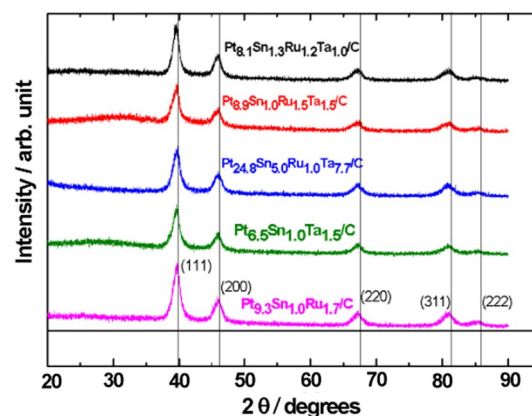

Fig. 1 XRD pattern of the PtSnRuTa/C electrocatalysts, KαCu ($\lambda = 1.5406$ Å) at room temperature, $2\theta = 10$–90° and step of 0.01° s^{-1}, JCPDS 04–802

All compositions showed a shift of the diffraction peaks to 2θ values lesser than concerning the fcc structure of pure Pt (Fig. 1). The behavior indicates that the crystalline lattice has been expanded; this is happening when the material forms a solid solution with atoms with larger atomic radius (Neto et al. 2005; Li et al. 2007). Therefore, this shift to 2θ values lesser suggests the formation of alloys with Sn (1.40 Å) and/or Ta (2.00 Å); as they have atomic radii greater than Pt (1.39 Å), the influence of Ru (1.34 Å) was not observed, because of having a smaller radius than the other metals (Reid et al. 2013; Crisafulli et al. 2014). The insertion of these atoms with greater atomic radius in the platinum crystalline lattice increases the interplanar distances, increasing in the lattice parameter (Table 1) to pure Pt ($a_{Pt} = 3.92$ Å, JCPDS 04-802), which confirms the expansion of the structure crystalline and alloy formation (Reid et al. 2013; Crisafulli et al. 2014). Therefore, the increase in the lattice parameter also increases the volume for all electrocatalysts investigated (Table 1) compared to pure Pt (60.38 Å^3, JCPDS 04-802). Moreover, the lattice parameter values observed in such material (3.943 Å to 3.949 Å) could also be related to the Pt_3Sn alloy ($a_{pt3Sn} = 4.00$ Å), thus considering the Sn^0 atomic radius (1.40 Å) one can infer that Sn atoms could form a substitutional solid solution, as observed before by us (Reid et al. 2013; Crisafulli et al. 2014).

The estimates of crystallite size (D) were obtained for each X-ray diffraction planes (111), (200), (220), and (311) using Scherrer's Eq. (1), considering that the nanoparticles are semi-spherical ($K = 0.9$). Furthermore, the increase in platinum loading results in the formation of particles of larger diameter (Ciapina et al. 2018), which justifies the D values found since the electrocatalysts have a 40% metallic loading with approximately 70% mol of Pt. Thus, the D values calculated for the electrocatalysts (3.8–9.8 nm) were consistent with the values already reported in the literature for Pt-based electrocatalysts synthesized using the same preparation method (Carrareto Caliman et al. 2013; Paganoto et al. 2017).

Energy-dispersive X-ray (EDX) results for the electrocatalysts investigated are also presented in Table 1, which indicates that each metal is present in a composition close to the nominal values, except for the quaternary $Pt_{24.8}Sn_{5.0}Ru_{1.0}Ta_{7.7}$/C electrocatalyst. A significant amount of oxygen (from 5.5 to 14% mol) was observed from the EDX measurements. The presence of oxygen may indicate the formation of metal oxides, even in a small amount, which may occur because calcination was performed in atmospheric air (Carrareto Caliman et al. 2013; Paganoto et al. 2017).

From transmission electron microscopy (TEM) images and histograms, Fig. 2, mean particle size values between 5.8 and 8.6 nm were obtained, consistent with the D values calculated from XRD (3.8–9.8 nm).

Images obtained using TEM and the histograms in Fig. 2 show that the electrocatalysts with Ta in their composition (for more details see Figure S2 in supplementary material) had more homogeneously dispersed nanoparticles on the surface of the Vulcan XC72 carbon. The nanoparticles of the $Pt_{9.3}Sn_{1.0}Ru_{1.7}$/C electrocatalyst show particle clusters, justifying their distribution more heterogeneously. Notably, the presence of clusters can decrease the area (Ciapina et al. 2013; Ferreira Frota et al. 2017). We have investigated the pure Pt/C electrocatalyst prepared using the DPP process (Evangelista et al. 2015), and we observed that the particle size ranged from 6.1 to 12.8 nm. Moreover, the particles were not well dispersed on Vulcan XC72 carbon. The higher particle density and particle size strongly suggest that nucleation is promoted on the Pt/C electrocatalyst, which leads to some undesirable agglomeration of the particles. Thus, we can infer that the quaternary electrocatalyst promotes better nanoparticle formation compared to pure Pt/C electrocatalyst.

Electrochemical characterization

Figure 3A shows the cyclic voltammogram representative of the PtSnRuTa/C system (*e.g.*, $Pt_{9.3}Sn_{1.0}Ru_{1.7}Ta_{0.0}$/C) obtained for different volumes (10 to 60 μL) of ink of the electrocatalytic material deposited on the polished surface of the glassy carbon working electrode with a 0.046

Table 1 Electrocatalysts obtained results by EDX and XRD analyses

Electrocatalysts		a	V	D[b]			
		Å	Å^3	Nm			
Nominal	Experimental[a]			(111)	(200)	(220)	(311)
$Pt_7Sn_1Ru_2$/C	$Pt_{9.3}Sn_{1.0}Ru_{1.7}$/C	3.945	61.4	7.3	5.8	6.6	5.3
$Pt_7Sn_1Ta_2$/C	$Pt_{6.5}Sn_{1.0}Ta_{1.5}$/C	3.943	61.3	9.8	6.6	6.9	5.9
$Pt_7Sn_1Ru_1Ta_1$/C	$Pt_{8.1}Sn_{1.3}Ru_{1.2}Ta_{1.0}$/C	3.947	61.5	5.5	5.4	6.9	5.9
$Pt_{14}Sn_2Ru_3Ta_1$/C	$Pt_{8.9}Sn_{1.0}Ru_{1.5}Ta_{1.5}$/C	3.949	61.6	4.5	3.9	3.8	4.2
$Pt_{14}Sn_2Ru_1Ta_3$/C	$Pt_{24.8}Sn_{5.0}Ru_{1.0}Ta_{7.7}$/C	3.943	61.3	8.6	6.0	6.5	5.9

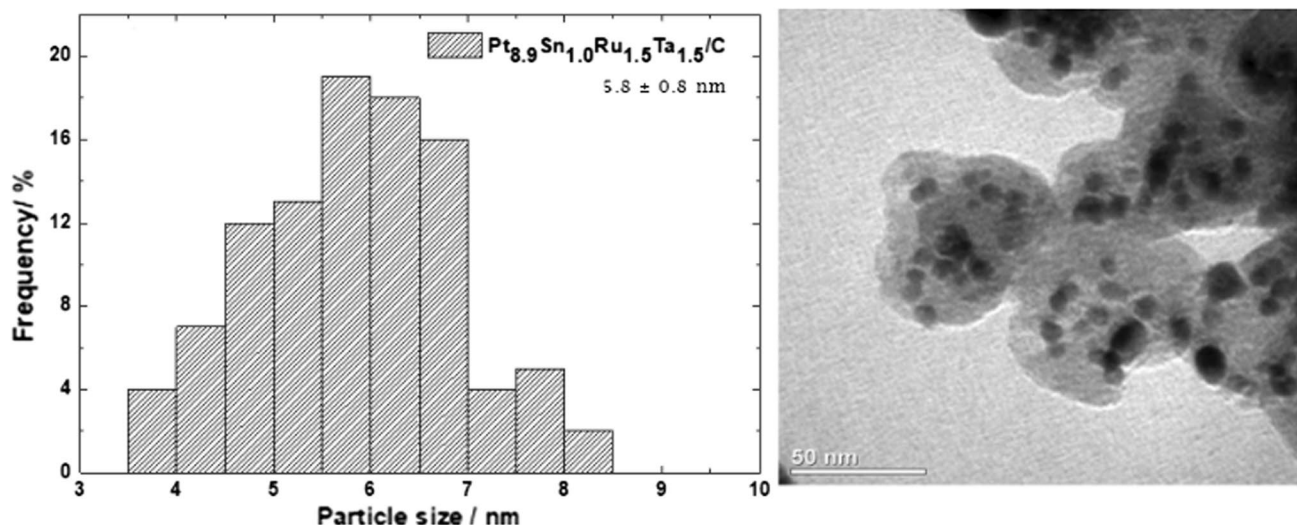[a]by EDX technique; [b]by XRD measurements; $a_{Pt} = 3.92$ Å; $a_{Pt3Sn} = 4.00$ Å

Fig. 2 Representative histogram and TEM image of the PtSnRuTa/C electrocatalysts

cm^2 geometric area. The voltammetric profile of the study electrocatalysts related to the reactions on the Pt surface is shown in Fig. 3A. In the positive-going potential scan, there is the hydrogen desorption region at −0.15 to 0.10 V *versus* Ag/AgCl, the double-layer charging region between 0.10 and 0.60 V *versus* Ag/AgCl, and Pt oxide formation from 0.6 V *versus* Ag/AgCl. In the negative-going potential scan, we reduce PtO to Pt at 0.8 to 0.2 V *versus* Ag/AgCl and adsorption of hydrogen on the metallic Pt surface at 0.1 to −0.1 V *versus* Ag/AgCl (Verma et al. 2021).

The results show that by increasing the volume of ink the electrocatalytic material deposited, the current increases, which was expected since there is an increase the material mass present on the working electrode (Ciapina et al. 2013). Furthermore, for small amounts of applied material (10–30 µL) good definition of the hydrogen adsorption/desorption peaks was obtained.

ECSA calculated from Eq. 4 was obtained from the hydrogen desorption peaks between −0.15 and 0.10 V *versus* Ag/AgCl, considering 210 µC cm^{-2} corresponds to the reference charge density necessary to promote the oxidation of a complete hydrogen monolayer (Binninger et al. 2014; Łukaszewski 2016). The highest ECSA obtained was 12.9 m^2 g$_{Pt}^{-1}$ for 20 uL of ink the electrocatalytic material. However, the results showed no significant increase in ECSA from 20 µL, probably due to the overlapping layers of the deposit of electrocatalytic material exposing the same number of active sites, leading to values close to the calculated areas (Easton and Pickup 2005). Thus, the glassy carbon working electrode used with a geometric area of 0.046 cm^2, 20 µL the volume of ink the electrocatalytic material, was considered ideal, aiming to define the voltammetric profile of ECSA better.

The cyclic voltammograms of Pt/C electrocatalysts modified with Sn, Ru, and Ta (Fig. 3B) exhibited behaviors similar to those already presented by Pt-based electrocatalysts and supported on carbon (Palma et al. 2014; Hidayati and Scott 2016). Among the five synthesized materials, the Pt$_{8.9}$Sn$_{1.0}$Ru$_{1.5}$Ta$_{1.5}$/C electrocatalyst showed higher current values normalized by the Pt loading. The increase in electrocatalytic activity (*i.e.,* current normalized) of this composition can be related to the synergistic effect of Ta and Ru. We have already investigated the binary PtSn/C electrocatalyst (Ribeiro et al. 2008; Artem et al. 2012), and one observed that the voltammograms did not display a well-defined hydrogen oxidation region, conversely to the case of PtSnRuTa/C system, and the current normalized in the double-layer region is larger than the showed here. Moreover, the beginning of the oxygen evolution reaction (OER) occurs at lower potentials for Pt$_{79}$Sn$_{21}$/C compared to PtSnRuTa/C system (Ribeiro et al. 2008). Recently, we also investigated the quaternary PtSnNiGa/C electrocatalysts (Santos et al. 2017a, b) and we observed a lower number of Pt active sites on the PtSnNiGa/C system because of cluster formation in these electrocatalysts. Moreover, the presence of other metals and oxides, such as Ni, Ga, NiOx, and GaOx species, may block the Pt active sites at low potentials as well (Assumpção et al. 2011). This behavior is not observed for the PtSnRuTa/C system.

Cyclic voltammetry was also used to observe changes in the voltammetric profile over 1000 cycles (*i.e.*, material stability) (Fig. 3C). With the increase in the number of cycles, we observed a reduction in the currents, and a change in the voltammetric profile, probably due to the restructuring of the catalyst by electrochemical stress and/or the loss of active sites. This loss of electroactivity can occur due
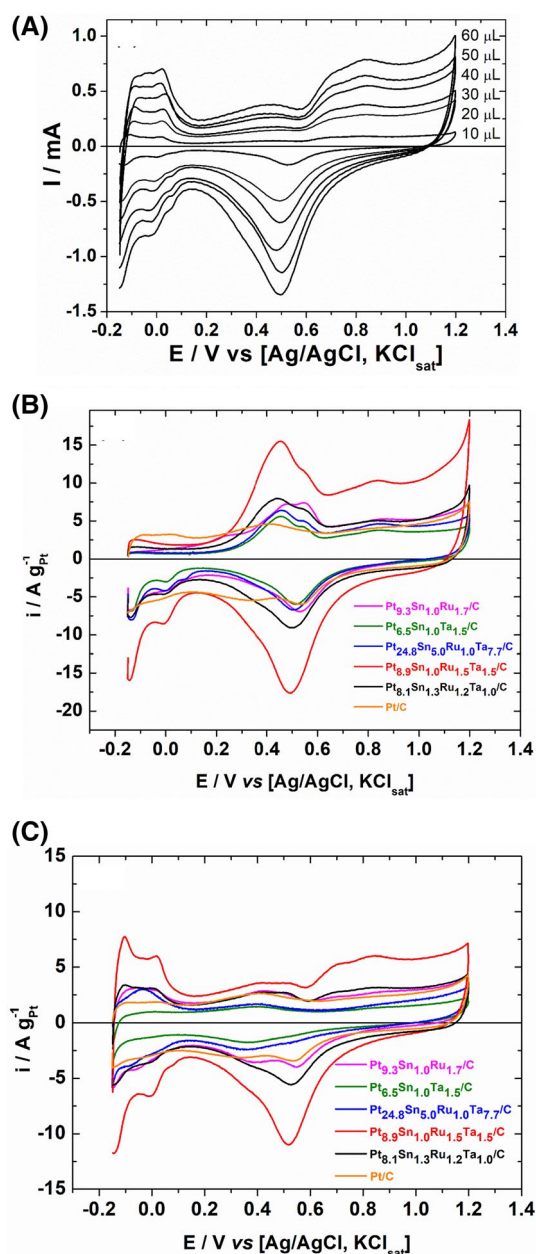
Fig. 3 **A** Cyclic voltammograms of the PtSnRuTa/C system using different volumes of ink of the electrocatalytic material on the working electrode. Cyclic voltammograms of the electrocatalysts containing Pt, Sn, Ru, and/or Ta, supported on Vulcan XC72 carbon for **B** 50 cycles and **C** 1000 cycles

Fig. 4 CO stripping voltammetry for electrocatalysts in H_2SO_4 0.5 mol L^{-1} after **A** 50 cycles and **B** 1000 cycles. **C** Comparison of ECSA values for 50 and 1000 cycles calculated from CO stripping voltammetry and hydrogen desorption charge

to particle agglomeration processes and the dissolution of metal/oxides (Easton and Pickup 2005; Zana et al. 2013). Although all compositions showed a reduction in the ECSA values (see Fig. 4C), the ternary electrocatalyst of composition $Pt_{6.5}Sn_{1.0}Ta_{1.5}/C$ showed a more significant loss in the definition of its voltammetric profile (see Fig. 3B and C) and, consequently, lower ECSA (1.3 m^2 g$_{Pt}^{-1}$) after 1000 cycles, reducing its corresponding area by 83% compared
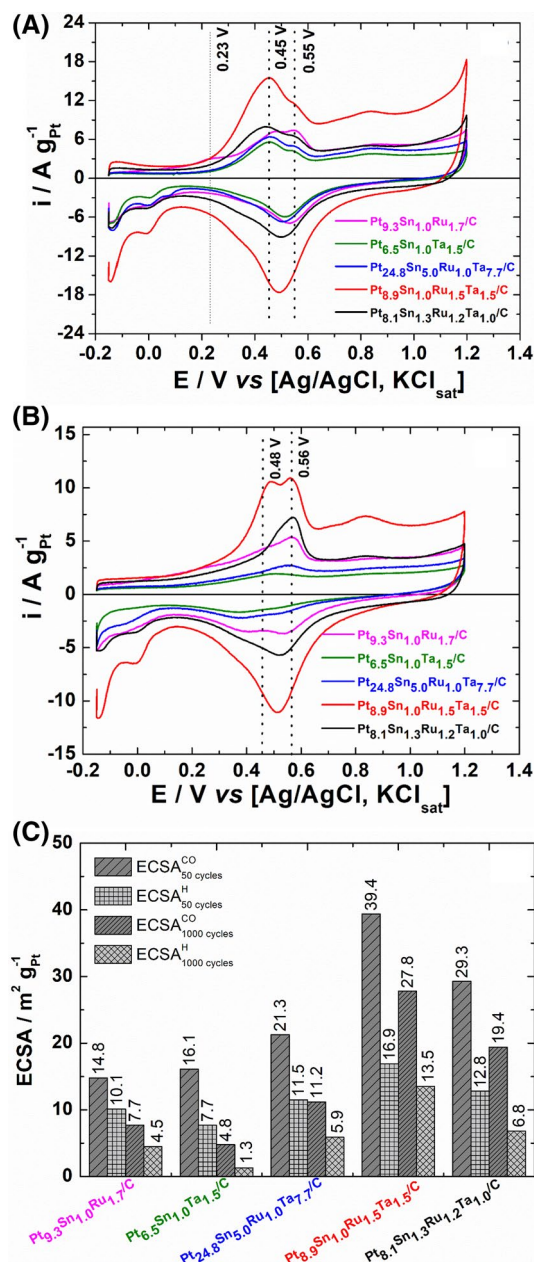
to the initial value of 7.7 m^2 g$_{Pt}^{-1}$. The second electrocatalyst that showed the most significant loss of ECSA was the $Pt_{9.3}Sn_{1.0}Ru_{1.7}/C$ ternary composition, which at the beginning of the experiment presented an ECSA of 10.1 m^2 g$_{Pt}^{-1}$ and at the end of the 1000 cycles, 4.5 m^2 g$_{Pt}^{-1}$, corresponding to 56% reduction, while the quaternary electrocatalysts $Pt_{8.9}Sn_{1.0}Ru_{1.5}Ta_{1.5}/C$ composition presents greater ECSA (16.9 m^2 g$_{Pt}^{-1}$) and lesser loss of ECSA, 20% (13.5 m^2 g$_{Pt}^{-1}$), at the end of the experiment. This composition also

showed higher stability of the voltammetric profile over the 1000 cycles, Fig. 3B and C. Additionally, the electrocatalysts showed a synergistic effect due to the addition of Ru and Ta since they had higher ECSA values (11.5 and 16.9 m^2 g$_{Pt}^{-1}$) than ternary electrocatalysts from 7.7 to 10.1 m^2 g$_{Pt}^{-1}$.

The cyclic voltammogram of the adsorbed CO oxidation of Fig. 4A shows that the electrocatalysts have different responses in terms of current normalized by the Pt loading, and the curve trend is not regular. For example, the Pt$_{8.9}$Sn$_{1.0}$Ru$_{1.5}$Ta$_{1.5}$/C electrocatalyst composition showed the highest peak current for CO oxidation, being the most electroactive among the synthesized electrocatalysts. The result is coherent with those observed in cyclic voltammetry in H$_2$SO$_4$ 0.5 mol L^{-1} (Fig. 4B), where the exact composition also showed a greater electroactive area. For the study of electrooxidation of methanol, it is possible to use carbon monoxide as a model since it has only one carbon (C1), and the produced intermediates in the reactions are common to both substances (Markovic 2002).

Therefore, with CO stripping measurements, the performance of electrocatalysts in the electrooxidation of type C1 molecules can be assessed in advance, as well as in the removal of poisons such as CO, which has a strong interaction with Pt sites and, consequently, decreases the performance of the materials (Scibioh et al. 2008; Arikan et al. 2013). The shape and position of the oxidation peak of the adsorbed CO can be related to the structure and composition of the electrocatalyst. Other factors such as the arrangement of diffraction planes on the crystallographic surface of the materials, the particle size and agglomeration, the type of support, type of supporting electrolyte, Pt content, and the presence of metals such as Sn, Ru, and Ta, can be correlated with the different shape of the CO peak (Massong et al. 2001; Arikan et al. 2013).

Figure 4A shows three characteristic peaks for CO oxidation relating to Pt$_{9.3}$Sn$_{1.0}$Ru$_{1.7}$/C electrocatalyst: two pre-peaks, one at 0.23 V and the other at 0.45 V and the main peak, more intense, at 0.55 versus Ag/AgCl. The presence of Sn and Ru has already been associated with the modification of peaks, leading to broader peaks with the presence of pre-peaks at smaller potentials (Santiago et al. 2004; Ribeiro et al. 2011). The reduction in the potential to oxidize CO occurs due to the greater availability of oxygenated species on the electrocatalyst surface, via a bifunctional mechanism, mainly due to the presence of Ru (Wiltshire et al. 2009; Masud et al. 2012). Additionally, due to the H$_2$O molecule's activation at low potentials, the interaction between OH and the adsorbed CO can lead to changes at the peak position. The behavior of electrocatalysts with Ta in their composition, Pt$_{6.5}$Sn$_{1.0}$Ta$_{1.5}$/C, Pt$_{24.8}$Sn$_{5.0}$Ru$_{1.0}$Ta$_{7.7}$/C, Pt$_{8.9}$Sn$_{1.0}$Ru$_{1.5}$Ta$_{1.5}$/C, and Pt$_{8.1}$Sn$_{1.3}$Ru$_{1.2}$Ta$_{1.0}$/C, showed similar curves for the oxidation of CO with the presence of two peaks, Fig. 4A, where the first and most intense potential

is at 0.45 V and a second less intense peak at 0.55 V versus Ag/AgCl.

All electrocatalysts showed a peak corresponding to the potential at 0.55 V versus Ag/AgCl, Fig. 4A. Peaks with higher CO oxidation potential are characteristic of the oxidation reaction in Pt sites with orientation (111) (Inkaew et al. 2008; López-Cudero et al. 2010). It is worth mentioning that this diffraction plane was the one that had the highest intensity in the XRD obtained results (Fig. 1). Thus, the peak of CO oxidation in the same potential for all quaternary electrocatalysts suggests that its oxidation occurred mainly at smaller potentials, but for the ternary based on Ru, the reaction prevailed on the Pt sites with orientation (111).

CO stripping voltammetry was also performed after 1000 cycles (Fig. 4B) to compare the ECSA values obtained from hydrogen desorption charge densities and evaluate the area between 50 and 1000 cycles (Fig. 4C). Observing Fig. 4C, the compositions Pt$_{24.8}$Sn$_{5.0}$Ru$_{1.0}$Ta$_{7.7}$/C, Pt$_{8.1}$Sn$_{1.3}$Ru$_{1.2}$Ta$_{1.0}$/C, and Pt$_{8.9}$Sn$_{1.0}$Ru$_{1.5}$Ta$_{1.5}$/C showed losses of initial ECSA to 47%, 33%, and 29%, respectively. These results confirm the greater stability of the quaternary electrocatalysts, as shown in Fig. 4B, C, where these compositions also showed less loss in the definition of the hydrogen desorption/adsorption peaks (see in supplementary material Figure S3 and S4) and higher ECSA values.

Throughout the 1000 cycles, it was observed that the potential for peak oxidation of CO was shifted to more positive values, as shown in Fig. 4B. This behavior confirms the loss of activity of the materials, since they need higher potentials to oxidize CO. This behavior can be explained due to the increase in particle size and by the metal dissolution (Arikan et al. 2013; Zana et al. 2013), leading to the loss of active sites, which was proven by the reduction of ECSA values.

Using the H$_2$SO$_4$ solution as a supporting electrolyte, the oxidation of CO adsorbed on Pt sites occurs via Langmuir–Hinshelwood mechanisms. Thus, the adsorbed CO reacts with oxygenated species present on the electrocatalyst surface, such as OH$^-$ or an activated water molecule (H$_2$O$_{ads}$) (Spendelow et al. 2004; Ciapina et al. 2018). Ru favors the activation of water molecules, which leads to the formation of oxygenated species on the electrocatalyst surface, aiding the oxidation and removal of CO on the active Pt sites (Ueda et al. 2003; González-Hernández et al. 2019). Ta and Sn have also been related to the bifunctional mechanism for assisting CO oxidation on Pt-based electrocatalysts (Maillard et al. 2004). Additionally, the presence of Ta can be associated with the electronic effects produced due to its interaction with the d orbitals of Pt, which leads to the weakening of the connection between CO and Pt, as already observed in other studies (Maillard et al. 2004). As shown in Fig. 4A, the electrochemical oxidation of CO was influenced by the Ta presence on the electrocatalysts, which resulted

in greater oxidation of CO at lower potentials, 0.45 V, than the electrocatalyst $Pt_{9.3}Sn_{1.0}Ru_{1.7}/C$, 0.55 V *versus* Ag/AgCl.

The ECSA results obtained from CO stripping voltammetry show values different from those calculated from the hydrogen desorption charge, Fig. 4C. This is reasonable because although the ECSA estimation procedure using hydrogen adsorption/desorption peaks at platinum sites is widely used for Pt-based electrocatalysts, it is not suitable for Pt-Ru electrocatalysts as there may be overlapping of OH adsorption processes occurring in Ru in the same potential range (Hadzi-Jordanov et al. 1977; Godoi et al. 2007). Furthermore, it can be seen that the ECSA of the ternary $Pt_{9.3}Sn_{1.0}Ru_{1.7}/C$ electrocatalyst was influenced by the method used. Probably it was caused by OH^- adsorption processes in Ru, as already mentioned.

Ternary $Pt_{6.5}Sn_{1.0}Ta_{1.5}/C$ and $Pt_{9.3}Sn_{1.0}Ru_{1.7}/C$ electrocatalysts, Fig. 4C, showed an 83% and 56% ECSA reduction, respectively. These results suggest that the addition of Ru and Ta to the electrocatalysts may cause a synergic effect on the PtSnM/C system. Related to quaternary electrocatalysts, an improvement was observed in the electrocatalyst response.

The cyclic voltammetry of the Pt/C electrocatalysts modified with Sn, Ru, and/or Ta for the electrooxidation of methanol, ethanol, ethylene glycol, and glycerol is depicted in Fig. 5A–D. The results indicate that the $Pt_{8.9}Sn_{1.0}Ru_{1.5}Ta_{1.5}/C$ quaternary electrocatalyst showed a more significant activity for the electrooxidation of the four study alcohols, providing a higher peak current (i_p) values by the Pt loading. The obtained results agree with the following characteristics: TEM, XRD, voltammetry on support electrolyte, and CO stripping, where the exact composition presented smaller crystallite size and particle size, and higher ECSA values too. Such results justify it is a more significant electrocatalytic activity against the oxidation of alcohols, due to the greater availability of active sites, favoring the electrooxidation process.

In cyclic voltammetry, all alcohols showed four peaks for oxidation, and such observation may be due to Sn, Ru, and Ta, which reaction intermediates at different potentials (Papageorgopoulos et al. 2002; Spendelow et al. 2004). Additionally, it can be observed a current increase in the oxidation of alcohols at a region potentials 1–1.2 V which can be attributed to the oxygen evolution
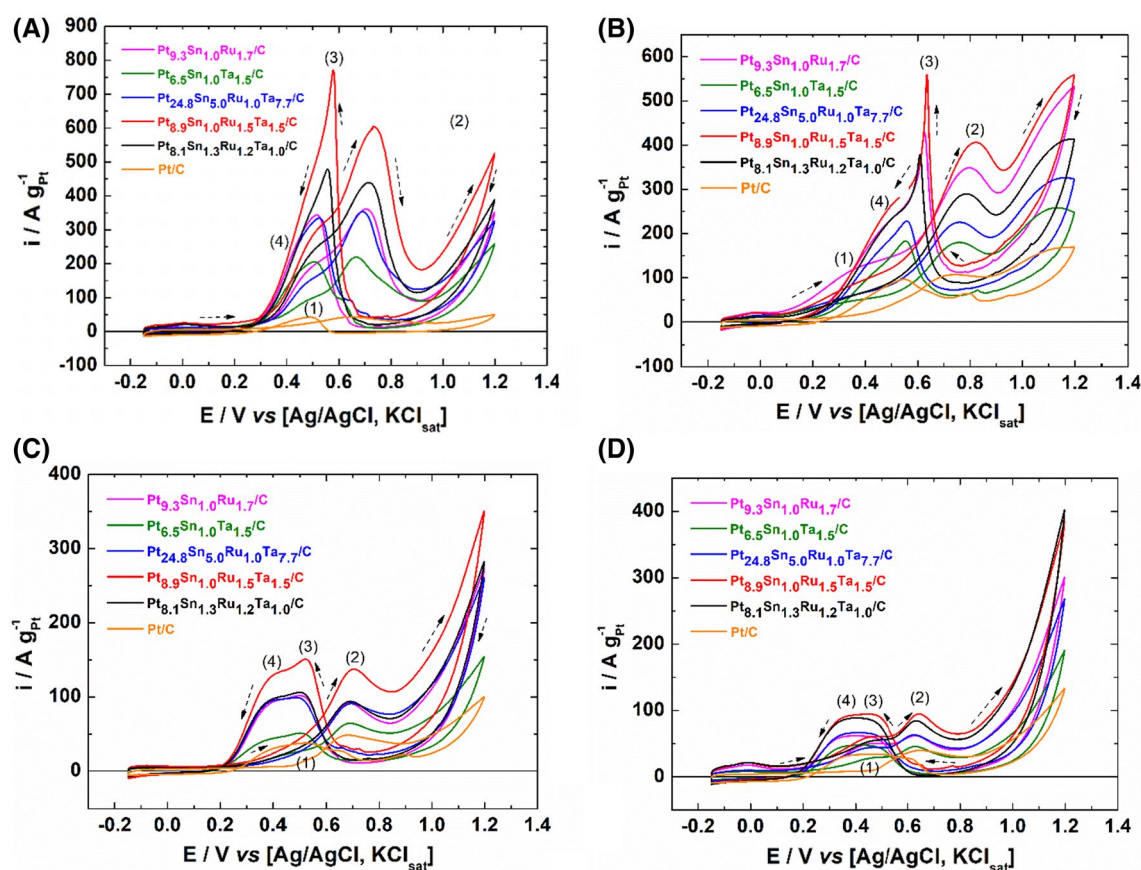

Fig. 5 Cyclic voltammograms from electrocatalysts in the presence of **A** methanol, **B** ethanol, **C** ethylene glycol, and **D** glycerol, 1.0 mol L^{-1} in H_2SO_4 0.5 mol L^{-1} with a scan rate of 20 mV s^{-1}

reaction. The oxidation peaks of methanol at 0.7 V on the positive-going potential scan (2) and at 0.5 V *versus* Ag/AgCl on the negative-going potential scan (3), shown in Fig. 5A, are already well known for Pt-based electrocatalysts (Justin et al. 2010; Ho et al. 2019). As from peaks 2 and 3, shown in Table 2, the ratio between currents (i_{p2}/i_{p3}) was calculated to assess tolerance to CO poisoning during methanol oxidation (Rahsepar et al. 2012; Mikkelsen et al. 2014; Ho et al. 2019). Thus, it was possible to find the ratios of 1.05 for the electrocatalysts $Pt_{9.3}Sn_{1.0}Ru_{1.7}/C$, $Pt_{6.5}Sn_{1.0}Ta_{1.7}/C$, and $Pt_{24.8}Sn_{5.0}Ru_{1.0}Ta_{7.7}/C$, respectively. For the electrocatalyst $Pt_{8.9}Sn_{1.0}Ru_{1.5}Ta_{1.5}/C$, it was 0.78, and for $Pt_{8.1}Sn_{1.3}Ru_{1.2}Ta_{1.0}/C$ 0.91. High values of this ratio indicate that methanol oxidation to CO_2 is dominant and that the remaining surface intermediates are negligible, indicating that the tested electrocatalyst is tolerant to poisoning by carbonaceous elements (Mikkelsen et al. 2014).

When comparing the activity of the electrocatalysts in relation to the alcohols understudy, as described in Table 2, methanol showed the highest activity in relation to the other alcohols, with higher currents normalized by Pt loading. The result was already expected due to the greater ease of the methanol oxidation process since it is a simple alcohol with

only one carbon atom and does not have a C–C bond, which is hard to cleave (Wang et al. 2001; Planes et al. 2007).

Regarding ethanol, the result obtained in this study was 12 times higher than the work of Queiroz e Ribeiro (Queiroz & Ribeiro 2019), where the maximum current normalized to EOR in a half-cell experiment was 43 A g_{Pt}^{-1} for the electrocatalyst $Pt_{75}Sn_{12}Ta_6Ru_7/C$, thus demonstrating that the material under study is promising for application in DEFC. For ethylene glycol, the material showed a less positive E_{onset} (0.39 V *vs.* Ag/AgCl) than reported by Zhao et al. (2019), where they reported a half-cell study of the Pd/Ta_2O_5-Pt electrode for the oxidation reaction of ethylene glycol with E_{onset} 0.39 V versus Ag/AgCl. A less positive E_{onset} is essential for better energy efficiency of the electrocatalyst. Thus, the electrocatalyst $Pt_{8.9}Sn_{1.0}Ru_{1.5}Ta_{1.5}/C$ shows its potential for applying DEGFC anodes. In the presence of glycerol, it is somewhat challenging to make an adequate comparison with the investigated electrocatalysts, since different experimental conditions obtained by Xin and Shen (Xin and Shen 2017), in a study, using doped fluor (F) and tantalum carbide partially oxidized carbon supported on graphite as an anodic electrocatalyst for glycerol oxidation reaction (GOR) showed an Eonset of 0.43 V versus SHE and a specific current of 24 mA cm^{-2} for a half-cell

Table 2 Currents and potentials of the oxidation peaks for all developed electrocatalysts

Oxidation Peaks									
Alcohols	Electrocatalysts	(1)			(2)		(3)		(4)	
		E_{onset}	E_1	I_{p1}	E_2	I_{p2}	E_3	I_{p3}	E_4	I_{p4}
		V		A g_{Pt}^{-1}	V	A g_{Pt}^{-1}	V	A g_{Pt}^{-1}	V	A g_{Pt}^{-1}
Methanol	$Pt_{9.3}Sn_{1.0}Ru_{1.7}/C$	0.31	0.49	196.6	0.70	361.5	0.51	342.5	0.39	184.6
	$Pt_{6.5}Sn_{1.0}Ta_{1.5}/C$	0.29	0.46	89.6	0.67	216.9	0.50	205.5	0.40	90.5
	$Pt_{8.9}Sn_{1.0}Ru_{1.5}Ta_{1.5}/C$	0.22	0.50	306.2	0.74	601.2	0.58	764.7	0.43	279.5
	$Pt_{8.1}Sn_{1.3}Ru_{1.2}Ta_{1.0}/C$	0.30	0.48	239.3	0.71	437.6	0.56	479.4	0.43	235.8
	$Pt_{24.8}Sn_{5.0}Ru_{1.0}Ta_{7.7}/C$	0.30	0.49	158.7	0.69	353.9	0.52	334.8	0.39	158.6
Ethanol	$Pt_{9.3}Sn_{1.0}Ru_{1.7}/C$	0.10	0.40	127.0	0.79	348.0	0.63	427.0	0.48	228.1
	$Pt_{6.5}Sn_{1.0}Ta_{1.5}/C$	0.17	0.40	52.4	0.76	180.2	0.55	183.5	0.46	128.2
	$Pt_{8.9}Sn_{1.0}Ru_{1.5}Ta_{1.5}/C$	0.14	0.40	92.7	0.82	406.6	0.63	539.6	0.49	256.6
	$Pt_{8.1}Sn_{1.3}Ru_{1.2}Ta_{1.0}/C$	0.20	0.40	65.7	0.79	289.4	0.61	381.3	0.49	225.2
	$Pt_{24.8}Sn_{5.0}Ru_{1.0}Ta_{7.7}/C$	0.15	0.40	65.4	0.76	225.5	0.56	226.1	0.44	159.6
Ethylene glycol	$Pt_{9.3}Sn_{1.0}Ru_{1.7}/C$	0.41	0.45	24.9	0.69	90.5	0.51	100.7	0.40	94.6
	$Pt_{6.5}Sn_{1.0}Ta_{1.5}/C$	0.41	0.45	23.2	0.69	63.7	0.51	51.1	0.40	45.0
	$Pt_{8.9}Sn_{1.0}Ru_{1.5}Ta_{1.5}/C$	0.38	0.44	33.5	0.70	137.6	0.51	150.4	0.40	130.1
	$Pt_{8.1}Sn_{1.3}Ru_{1.2}Ta_{1.0}/C$	0.41	0.45	24.8	0.69	94.4	0.50	106.8	0.40	97.7
	$Pt_{24.8}Sn_{5.0}Ru_{1.0}Ta_{7.7}/C$	0.46	0.46	19.5	0.69	90.6	0.50	98.7	0.40	95.7
Glycerol	$Pt_{9.3}Sn_{1.0}Ru_{1.7}/C$	0.32	0.48	50.9	0.63	61.1	0.45	61.6	0.37	59.9
	$Pt_{6.5}Sn_{1.0}Ta_{1.5}/C$	0.42	0.50	30.3	0.63	45.7	0.44	47.9	0.36	44.5
	$Pt_{8.9}Sn_{1.0}Ru_{1.5}Ta_{1.5}/C$	0.26	0.48	61.1	0.64	95.0	0.44	94.2	0.37	90.7
	$Pt_{8.1}Sn_{1.3}Ru_{1.2}Ta_{1.0}/C$	0.27	0.49	55.0	0.63	84.7	0.43	89.0	0.37	87.3
	$Pt_{24.8}Sn_{5.0}Ru_{1.0}Ta_{7.7}/C$	0.30	0.48	51.9	0.64	80.6	0.45	66.8	0.37	63.3

experiment in cyclic voltammetry. Xin and Shen (Xin and Shen 2017) showed a much more positive charge distributed around Ta in the electrocatalyst than in other metals, which favored the chemisorption of O with the negative charge of alcohol and weakened the binding force of CO, which in turn facilitated the GOR kinetics. However, the E_{onset} (0.46 V vs. SHE) obtained in this study was similar to that reported by them. In this way, we continue to improve the Ta-modified electrocatalysts for DGFC.

In the quaternary electrocatalysts, the results of the electrooxidation of alcohols corroborate with the results previously reported, such as ECSA. The electrocatalytic activity increases in this way: $Pt_{24.8}Sn_{5.0}Ru_{1.0}Ta_{7.7}/C < Pt_{8.1}Sn_{1.3}Ru_{1.2}Ta_{1.0}/C < Pt_{8.9}Sn_{1.0}Ru_{1.5}Ta_{1.5}/C$.

The synergistic effect between Ru and Ta increased current density values from about 40% to 50% for the oxidation of all alcohols. The increase in the peak current due to Ru and Ta probably occurred due to the increase in ECSA values, but it is also related to the bifunctional and electronic effects that can occur due to the presence of these metals (Planes et al. 2007).

Comparing the values of potential oxidation onset (E_{onset}) obtained for the different alcohols in Table 2, it was observed that the electrocatalysts had lower E_{onset} for methanol and ethanol, indicating the metals addition in question it was best evidenced by the increased electrocatalytic activity in these alcohols. Lower E_{onset} values indicate a lesser amount of energy needed to promote the electrooxidation of alcohols, making it easier for the reaction to start, which can be attributed to the presence of metals Sn, Ru, and Ta, where the bifunctional mechanism and electronic effect increase the presence of oxygenated species in addition to altering the interaction of oxidation intermediates on the material surface (Masud et al. 2012; Queiroz and Ribeiro 2019).

The curves obtained from the chronoamperometric measurements of alcohols showed a decrease in the current values as the alcohol oxidation reaction progresses, as shown in Fig. 6. This happens due to the oxidation reaction intermediates accumulating on the electrocatalyst surface, preventing new molecules from being oxidized.

In methanol, the composition $Pt_{8.9}Sn_{1.0}Ru_{1.5}Ta_{1.5}/C$ showed divergent results compared to other alcohols. This composition showed the highest current values at the beginning and up to approximately 90 min of reaction. However, it was the one that exhibited the most remarkable drop in current, suggesting less stability in methanol oxidation.
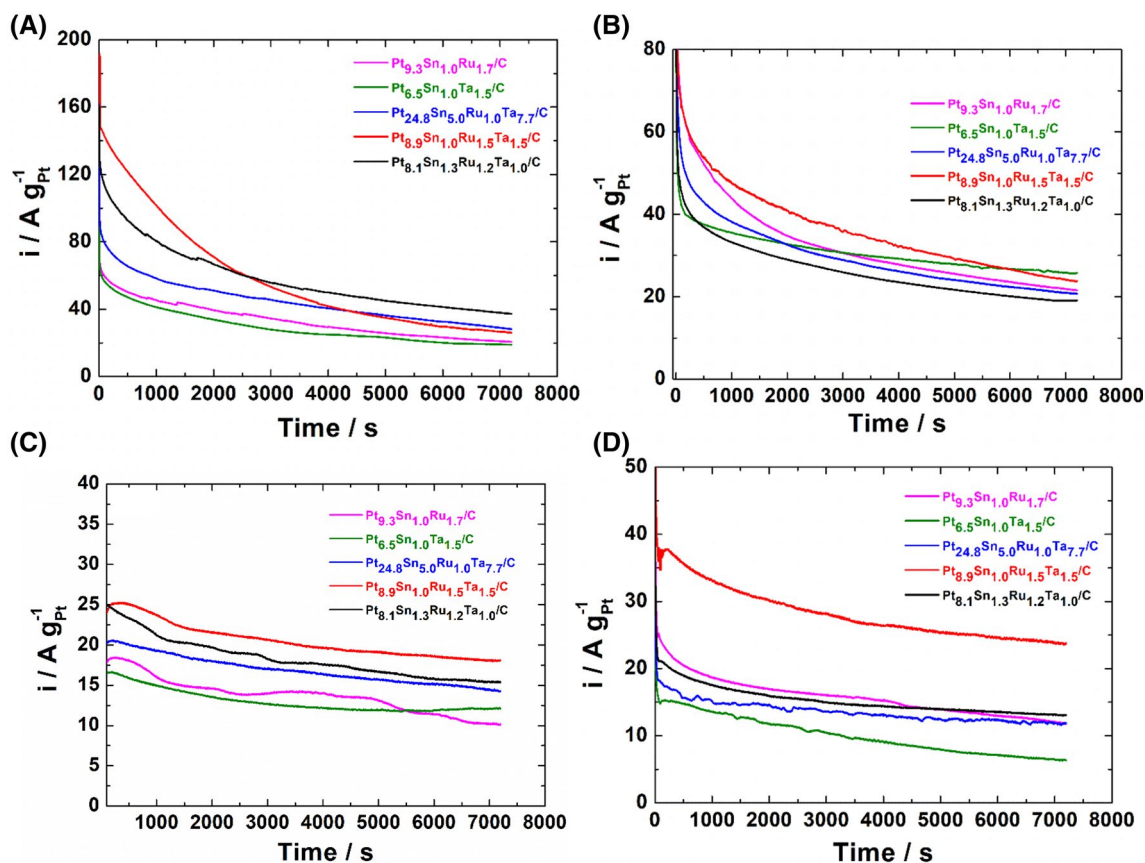

Fig. 6 Chronoamperometry curves in **A** methanol, **B** ethanol, **C** ethylene glycol, and **D** glycerol for all developed electrocatalysts

This result corroborates the voltammetry measurements in methanol, in which, despite this composition showing more significant electrocatalytic activity, it was also the one that showed less tolerant of CO poisoning. As in the oxidation of methanol, CO represents an intermediate; its presence led to a more significant drop in current, as seen in the measurements in ethanol-related to $Pt_{8.9}Sn_{1.0}Ru_{1.5}Ta_{1.5}/C$ showed the lowest current variation (6.0 A g_{Pt}^{-1}) at the end of 2 h, becoming the most stable and with the most significant electrocatalytic activity in this alcohol. Comparing the obtained current results at the end of the experiment, the values obtained for the electrocatalysts (19–26 A g_{Pt}^{-1}) were higher than those of the binary PtSn/C (Tayal et al. 2011; Almeida et al. 2012) electrocatalysts with the same Pt content (70% mol) and PtRu/C (Sudachom et al. 2017) with 45% and 20% of metal.

The obtained results in this study, in terms of current, are promising if compared to some literature studies on ternary PtSnRu/C electrocatalysts (0.6–5 A g_{Pt}^{-1}) (Mikkelsen et al. 2014). In fact, the current values are higher than references (Mikkelsen et al. 2014), showing that the insertion of Ta on the PtSnRu/C electrocatalysts increased their electrocatalytic activity and the ability to renew the electrocatalytic surface due to current stability throughout the test.

The results for ethylene glycol and glycerol were similar for the $Pt_{8.9}Sn_{1.0}Ru_{1.5}Ta_{1.5}/C$ electrocatalyst, which obtained higher current values at a steady state after 2 h, as shown in Fig. 6C and D. In addition, this composition also showed the smallest reduction in current values in the first seconds of the experiment, which can be attributed to the greater tolerance of the electrocatalyst to poisoning by oxidation reaction intermediates.

Unlike the results in ethanol, the ternary composition with Ta ($Pt_{6.5}Sn_{1.0}Ta_{1.7}/C$) in the presence of ethylene glycol and glycerol did not show good activity for the oxidation of these alcohols since their current values were the lowest among the other synthesized electrocatalysts, as shown in Fig. 6C and D. The obtained results in ethanol, ethylene glycol, and glycerol showed that the electrocatalyst composition $Pt_{8.9}Sn_{1.0}Ru_{1.5}Ta_{1.5}/C$ had a higher activity for the oxidation of these alcohols. According to Xin et al.(Polonský et al. 2012), tantalum-modified electrocatalysts have a more extensive positive charge distribution than Pt, Sn, and Ru. This positive charge favors the adsorption of oxygen from alcohol molecules due to the negative charge on oxygen. This phenomenon may be a reason for the improvement observed here in electrocatalysts modified with tantalum. It is worth mentioning from previous results that this composition showed smaller crystallite size, better activity in acid medium, and higher ECSA values, presenting better activity and stability for the oxidation of these same alcohols.

Table 3 Values of potential obtained during electrolysis at 15 h with a current density of 3 mA cm^{-2} in the presence of methanol, ethanol, ethylene glycol, and glycerol potential and ECSA to CO and H from chronoamperometric for all electrocatalysts investigated

Alcohols	Electrocatalysts	E_i	E_f	E_f–E_i	Chrono-ampero-metric	ECSA^{CO}	ECSA^H
		V vs Ag/AgCl	V	A g_{Pt}^{-1}		A m^2	
Methanol	$Pt_{9.3}Sn_{1.0}Ru_{1.7}/C$	0.27	0.98	0.71	20.67	2.68	4.59
	$Pt_{6.5}Sn_{1.0}Ta_{1.5}/C$	0.25	0.39	0.14	18.87	3.93	14.52
	$Pt_{8.9}Sn_{1.0}Ru_{1.5}Ta_{1.5}/C$	0.27	0.50	0.23	26.06	0.94	1.93
	$Pt_{8.1}Sn_{1.3}Ru_{1.2}Ta_{1.0}/C$	0.26	0.97	0.37	37.37	1.93	5.50
	$Pt_{24.8}Sn_{5.0}Ru_{1.0}Ta_{7.7}/C$	0.31	0.90	0.59	18.34	1.64	3.11
Ethanol	$Pt_{9.3}Sn_{1.0}Ru_{1.7}/C$	0.16	0.32	0.16	21.57	2.80	4.79
	$Pt_{6.5}Sn_{1.0}Ta_{1.5}/C$	0.24	0.43	0.19	25.68	5.35	19.75
	$Pt_{8.9}Sn_{1.0}Ru_{1.5}Ta_{1.5}/C$	0.08	0.17	0.09	23.77	0.86	1.76
	$Pt_{8.1}Sn_{1.3}Ru_{1.2}Ta_{1.0}/C$	0.20	0.38	0.18	19.10	0.98	2.81
	$Pt_{24.8}Sn_{5.0}Ru_{1.0}Ta_{7.7}/C$	0.16	0.33	0.17	20.78	1.86	3.52
Ethylene glycol	$Pt_{9.3}Sn_{1.0}Ru_{1.7}/C$	0.30	0.36	0.06	10.16	1.32	2.26
	$Pt_{6.5}Sn_{1.0}Ta_{1.5}/C$	0.28	0.35	0.07	12.18	2.54	9.37
	$Pt_{8.9}Sn_{1.0}Ru_{1.5}Ta_{1.5}/C$	0.28	0.34	0.06	18.12	0.65	1.34
	$Pt_{8.1}Sn_{1.3}Ru_{1.2}Ta_{1.0}/C$	0.31	0.93	0.62	15.40	0.79	2.26
	$Pt_{24.8}Sn_{5.0}Ru_{1.0}Ta_{7.7}/C$	0.35	0.49	0.14	14.24	1.27	2.41
Glycerol	$Pt_{9.3}Sn_{1.0}Ru_{1.7}/C$	0.22	0.28	0.06	11.80	1.53	2.62
	$Pt_{6.5}Sn_{1.0}Ta_{1.5}/C$	0.27	0.34	0.07	6.40	1.33	4.92
	$Pt_{8.9}Sn_{1.0}Ru_{1.5}Ta_{1.5}/C$	0.20	0.24	0.04	23.57	0.85	1.75
	$Pt_{8.1}Sn_{1.3}Ru_{1.2}Ta_{1.0}/C$	0.28	0.33	0.05	13.17	0.68	1.94
	$Pt_{24.8}Sn_{5.0}Ru_{1.0}Ta_{7.7}/C$	0.24	0.30	0.06	11.87	1.06	2.01

The current results in the chronoamperometry experiment (Fig. 6) were also normalized by ECSA for CO and H, as shown in Table 3. It is possible to observe that the highest current densities are associated with the electrocatalyst ternary $Pt_{6.5}Sn_{1.0}Ta_{1.5}/C$ for all alcohols investigated, for both $ECSA^{CO}$ and $ECSA^H$ (Table 3). This result is an indication that Ta promotes an increase in electrocatalytic activity due to a bifunctional mechanism and electronic effect (Ottoni et al. 2016; Souza et al. 2021).

To evaluate the electrocatalytic activity of electrocatalysts against the electrooxidation of alcohols, chronopotentiometry experiments were performed as shown in Fig. 7 and summarized in Table 3, respectively. The oscillatory behavior observed in the chronopotentiometry curves is related to the presence of CO_{ads} molecules formed during oxidation (Wang et al. 2001; Delmonde et al. 2014).

From the results obtained regarding the methanol electrooxidation indicated in Fig. 7a, we observed that the electrocatalysts of compositions $Pt_{9.3}Sn_{1.0}Ru_{1.7}/C$, $Pt_{8.1}Sn_{1.3}Ru_{1.2}Ta_{1.0}/C$, and $Pt_{24.8}Sn_{5.0}Ru_{1.0}Ta_{7.7}/C$ showed an increase in potential at different time intervals; such behavior implies the degradation of the electrocatalytic

material, leading to its activity loss (Wang et al. 2001; Delmonde et al. 2014). The compositions $Pt_{6.5}Sn_{1.0}Ta_{1.5}/C$ and $Pt_{8.9}Sn_{1.0}Ru_{1.5}Ta_{1.5}/C$ showed constant curves above 15 h, being less susceptible to surface poisoning. The electrocatalysts in the presence of ethanol, Fig. 7b, and ethylene glycol, Fig. 7c, showed similar behavior, differing only in the presence of the compositions $Pt_{8.9}Sn_{1.0}Ru_{1.5}Ta_{1.5}/C$, which showed a potential increase after 10 h of experiment. For glycerol, Fig. 7d, the chronopotentiometry profile did not show an oscillatory potential characteristic, as shown for pure Pt in the presence of H_2SO_4 (Oliveira et al. 2012). Regarding the electrooxidation of alcohols against the stability of the materials under study, shown in Table 3, the electrocatalysts showed better stability during the electrooxidation of glycerol, exhibiting small variations from 0.06 to 0.07 vs. Ag/AgCl.

In the electrooxidation of methanol, oscillatory behavior occurs due to CO formation, absorbed in the Pt active sites by deactivating them. Therefore, constant potential increases are needed to reactivate the active catalytic sites (Huang et al. 2009; Silva et al. 2019). Under the conditions studied in chronopotentiometry, the $Pt_{6.5}Sn_{1.0}Ta_{1.5}/C$
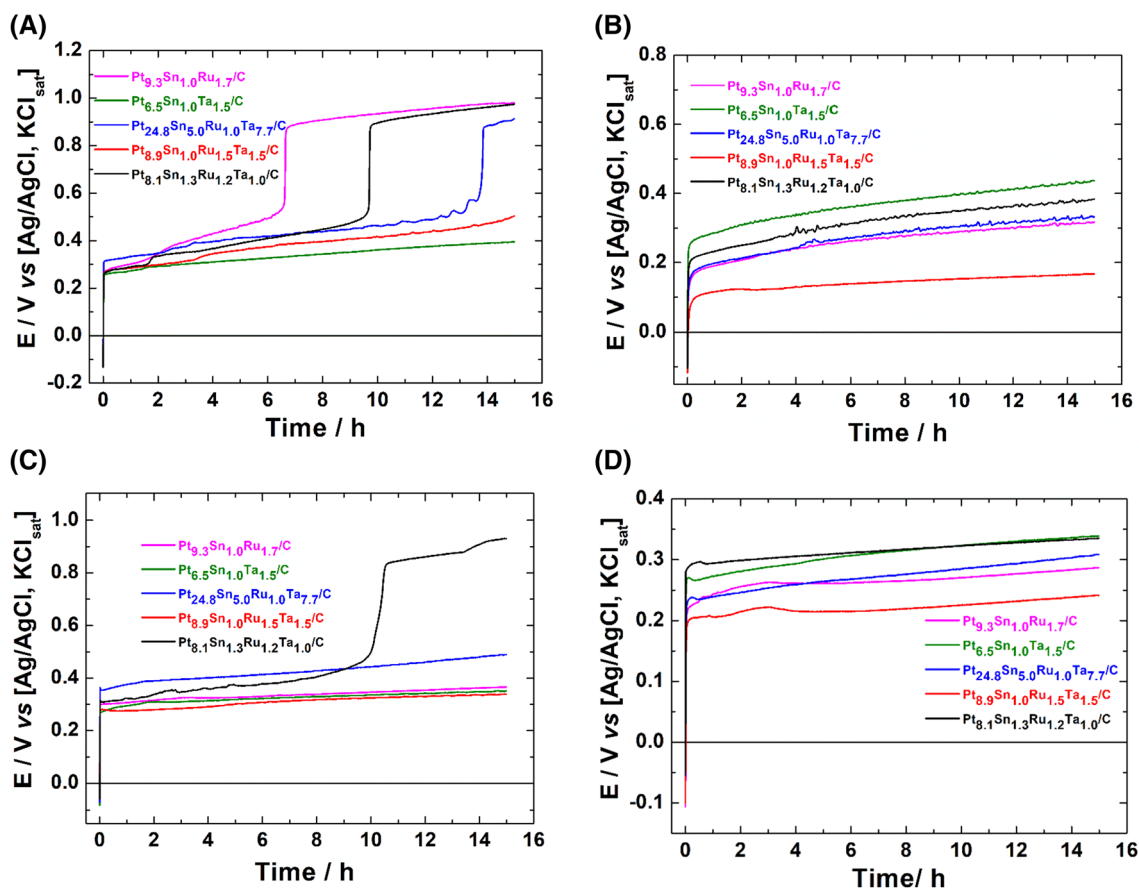

Fig. 7 Chronopotentiometry measurements in **A** methanol, **B** ethanol, **C** ethylene glycol, and **D** glycerol for all developed electrocatalysts in H_2SO_4 0.5 mol L^{-1} with a current density of 3 mA cm^{-2} for 15 h

and $Pt_{8.9}Sn_{1.0}Ru_{1.5}Ta_{1.5}$/C electrocatalysts showed constant curves throughout the 15 h, being less susceptible to the poisoning of its surface, therefore more stable due to their smaller potential variations, 0.14 and 0.23 V *versus* Ag/AgCl, respectively (Table 3). Such results again show the contribution of Ta, leading to increased material stability.

In ethanol and glycerol, the electrocatalysts present curves without a sudden increase in potential. However, minor potential variations were obtained in these two alcohols for the $Pt_{8.9}Sn_{1.0}Ru_{1.5}Ta_{1.5}$/C electrocatalyst, 0.09 and 0.04 *versus* Ag/AgCl, respectively. Furthermore, the results of chronopotentiometry curves were consistent with those of chronoamperometry, showing that for these alcohols, the synergistic effect of Ru and Ta improved the electrocatalytic activity and the tolerance for the products formed in the electrooxidation (Almeida et al. 2013).

The results of the electrocatalysts in ethylene glycol were also consistent with the chronoamperometry because the $Pt_{8.9}Sn_{1.0}Ru_{1.5}Ta_{1.5}$/C electrocatalyst showed better results. However, unlike the other electrocatalysts, the composition $Pt_{8.1}Sn_{1.3}Ru_{1.2}Ta_{1.0}$/C showed an increase at potential after 10 h of the experiment but did not show stationary behavior, that is, lower electrocatalytic activity in the ethylene glycol compared to the other electrocatalysts, since it needed greater potentials to maintain the current (Sitta et al. 2010).

The observed increase in the oxidation of small organic molecules due to Ta as a cocatalyst and PtSnRu was associated with a strong interaction between Ta and Pt, resulting in electron donation from Pt to Ta, as seen before by us (Queiroz and Ribeiro 2019). This donation causes a positive charge distribution on the Pt surface, and this positive charge on the Pt weakens the binding strength of the adsorbed CO at the Pt sites (Masud et al. 2012). In this way, the ability to remove intermediates adsorbed on Pt is increased. Therefore, the main properties that Ta can improve Pt catalysts' performance for alcohol oxidation are mainly related to positive charge distribution on Pt, the performance of the bifunctional mechanism (Souza et al. 2020), and the electronic effect (Artem et al. 2012).

Conclusions

The XRD results indicated the incorporation of metal Ta into the Pt structure, increasing in the crystalline lattice and increasing volume. TEM results showed good dispersion of the electrocatalysts on the carbon support. To evaluate the influence of the volume of ink of the electrocatalytic material added to the working electrode was studied, verifying that volumes above 30 μL do not increase the electrochemically active surface area (ECSA). In cyclic voltammetry in the presence of alcohols, the electrocatalyst $Pt_{8.9}Sn_{1.0}Ru_{1.5}Ta_{1.5}$/C was the one that showed the best

electrocatalytic activity for all alcohols, a result expected since this electrocatalyst had a smaller particle size and higher ECSA value. In chronoamperometry and chronopotentiometry studies, the $Pt_{8.9}Sn_{1.0}Ru_{1.5}Ta_{1.5}$/C electrocatalyst showed better results in ethanol, ethylene glycol, and glycerol. This result can be related to the electronic effect observed also in the CO stripping voltammetry favored by the presence of Ta and Sn, which can decrease the adsorption of the intermediates on the Pt sites, allowing a constant renewal of the electrocatalytic surface.

References

Almeida TS, Palma LM, Leonello PH, Morais C, Kokoh KB, De Andrade AR (2012) An optimization study of PtSn/C catalysts applied to direct ethanol fuel cell: effect of the preparation method on the electrocatalytic activity of the catalysts. J Power Sources 215:53–62

Almeida TS, Palma LM, Morais C, Kokoh KB, De Andrade AR (2013) Effect of adding a third metal to carbon-supported PtSn-based nanocatalysts for direct ethanol fuel cell in acidic medium. J Electrochem Soc 160:F965–F971

Arikan T, Kannan AM, Kadirgan F (2013) Binary Pt–Pd and ternary Pt–Pd–Ru nanoelectrocatalysts for direct methanol fuel cells. Int J Hydrogen Energy 38:2900–2907

Artem LM, Santos DM, De Andrade AR, Kokoh KB, Ribeiro J (2012) Development of ternary and quaternary catalysts for the electrooxidation of glycerol. Sci World J 2012:1–6

Assumpção MHMT, De Souza RFB, Rascio DC, Silva JCM, Calegaro ML, Gaubeur I, Paixão TRLC, Hammer P, Lanza MRV, Santos MC (2011) A comparative study of the electrogeneration of hydrogen peroxide using Vulcan and Printex carbon supports. Carbon n y 49:2842–2851

Awaludin Z, Suzuki M, Masud J, Okajima T, Ohsaka T (2011) Enhanced electrocatalysis of oxygen reduction on Pt/TaO x/GC. J Phys Chem C 115:25557–25567

Badwal SPS, Giddey S, Kulkarni A, Goel J, Basu S (2015) Direct ethanol fuel cells for transport and stationary applications–a comprehensive review. Appl Energy 145:80–103

Basha SA, Gopal KR, Jebaraj S (2009) A review on biodiesel production, combustion, emissions and performance. Renew Sustain Energy Rev 13:1628–1634

Binninger T, Fabbri E, Kötz R, Schmidt TJ (2014) Determination of the electrochemically active surface area of metal-oxide supported platinum catalyst. J Electrochem Soc 161:H121–H128

Breeze P (2019) Power generation technologies, 3rd ed, Power Generation Technologies. Elsevier, United Kingdom.

Carrareto Caliman C, Palma LM, Ribeiro J (2013) Evaluation of Ni and Ti addition in PtSn/C catalysts for ethanol and glycerol electrooxidation. J Electrochem Soc 160:F853–F858

Ciapina EG, Santos SF, Gonzalez ER (2013) The electro-oxidation of carbon monoxide and ethanol on supported Pt nanoparticles: the influence of the support and catalyst microstructure. J Solid State Electrochem 17:1831–1842

Ciapina EG, Santos SF, Gonzalez ER (2018) Electrochemical CO stripping on nanosized Pt surfaces in acid media: a review on the issue of peak multiplicity. J Electroanal Chem 815:47–60

Cohen JL, Volpe DJ, Abruña HD (2007) Electrochemical determination of activation energies for methanol oxidation on polycrystalline platinum in acidic and alkaline electrolytes. Phys Chem Phys 9:49–77

Crisafulli R, Antoniassi RM, Oliveira Neto A, Spinacé EV (2014) Acid-treated PtSn/C and PtSnCu/C electrocatalysts for ethanol electro-oxidation. Int J Hydrogen Energy 39:5671–5677

Delmonde MVF, Nascimento MA, Nagao R, Cantane DA, Lima FHB, Varela H (2014) Production of volatile species during the oscillatory electro-oxidation of small organic molecules. J Phys Chem C 118(31):17699–17709

Dimakis N, Cowan M, Hanson G, Smotkin ES (2009) Attraction−repulsion mechanism for carbon monoxide adsorption on platinum and platinum−ruthenium alloys. J Phys Chem C 113:18730–18739

dos Santos MC, Parreira LS, De Moura Souza F, Camargo Junior J and Gentil T, (2017b) Fuel cells: hydrogen and ethanol technologies, In: (editor-in-chief), S.H. (Ed.), Reference module in materials science and materials engineering. Elsevier, Santo André, Brazil, pp. 1–22.

Easton EB, Pickup PG (2005) An electrochemical impedance spectroscopy study of fuel cell electrodes. Electrochim Acta 50:2469–2474

El Attar A, Oularbi L, Chemchoub S, El Rhazi M (2020) Preparation and characterization of copper oxide particles/polypyrrole (Cu2O/PPy) via electrochemical method: application in direct ethanol fuel cell. Int J Hydrogen Energy 45:8887–8898

Evangelista TCS, Paganoto GT, Guimarães MCC, Ribeiro J (2015) Raman spectroscopy and electrochemical investigations of Pt electrocatalyst supported on carbon prepared through plasma pyrolysis of natural gas. J Spectrosc 2015:1–7

Ferreira Frota E, Silva de Barros VV, de Araújo BRS, Gonzaga Purgatto Â, Linares JJ (2017) Pt/C containing different platinum loadings for use as electrocatalysts in alkaline PBI-based direct glycerol fuel cells. Int J Hydrogen Energy 42:23095–23106

Fujiwara N, Siroma Z, Yamazaki S, Ioroi T, Senoh H, Yasuda K (2008) Direct ethanol fuel cells using an anion exchange membrane. J Power Sources 185:621–626

Godoi DRM, Perez J, Mercedes Villullas H (2007) Influence of particle size on the properties of Pt–Ru/C catalysts prepared by a microemulsion method. J Electrochem Soc 154:B474

González-Hernández M, Antolini E, Perez J (2019) Synthesis, characterization and CO tolerance evaluation in PEMFCs of Pt2RuMo electrocatalysts. Catalysts 9:61

Gregoire JM, Tague ME, Cahen S, Khan S, Abruña HD, DiSalvo FJ, van Dover RB (2010) Improved fuel cell oxidation catalysis in Pt 1−x Ta x. Chem Mater 22:1080–1087

Hadzi-Jordanov S, Angerstein-Kozlowska H, Vukovic M, Conway BE (1977) The state of electrodeposited hydrogen at ruthenium electrodes. J Phys Chem 81:2271–2279

Hidayati N, Scott K (2016) Electro-oxidation of ethanol on carbon supported PtSn and PtSnNi catalysts. Bull Chem React Eng Catal 11:10

Ho VTT, Pham HQ, Anh THT, Van Nguyen A, Quoc KAN, Vo HTH, Nguyen TT (2019) Highly stable Pt/ITO catalyst as a promising electrocatalyst for direct methanol fuel cells. Comptes Rendus Chim 22:838–843

Huang T, Liu J, Li R, Cai W, Yu A (2009) A novel route for preparation of PtRuMe (Me=Fe Co, Ni) and their catalytic performance for methanol electrooxidation. Electrochem Commun 11:643–646

Huber GW, Iborra S, Corma A (2006) Synthesis of transportation fuels from biomass: chemistry, catalysts, and engineering. Chem Rev 106:4044–4098

Inkaew P, Zhou W, Korzeniewski C (2008) CO monolayer oxidation at Pt(100) probed by potential step measurements in comparison to Pt(111) and Pt nanoparticle catalyst. J Electroanal Chem 614:93–100

Justin P, Hari Krishna Charan P and Ranga Rao G (2010) High performance Pt–Nb2O5/C electrocatalysts for methanol electrooxidation in acidic media. Appl Catal B Environ 100, 510–515

Kakinuma K, Hirayama N, Iiyama A, Watanabe M, Uchida M (2017) Electrochemical oxidation of hydrolyzed poly-oxymethylenedimethylether by Pt and PtRu catalysts on ta-doped SnO 2 supports for direct oxidation fuel cells. J Electrochem Soc 164:F1226–F1233

Kim HJ, Choi SM, Green S, Tompsett GA, Lee SH, Huber GW, Kim WB (2011) Highly active and stable PtRuSn/C catalyst for electrooxidations of ethylene glycol and glycerol. Appl Catal B Environ 101:366–375

Li C, Baek J-B (2020) Recent advances in noble metal (Pt, Ru, and Ir)-based electrocatalysts for efficient hydrogen evolution reaction. ACS Omega 5:31–40

Li H, Sun G, Cao L, Jiang L, Xin Q (2007) Comparison of different promotion effect of PtRu/C and PtSn/C electrocatalysts for ethanol electro-oxidation. Electrochim Acta 52:6622–6629

Liu L, Huang Z, Wang D, Scholz R, Pippel E (2011) The fabrication of nanoporous Pt-based multimetallic alloy nanowires and their improved electrochemical durability. Nanotechnology 22:105604

López-Cudero A, Solla-Gullón J, Herrero E, Aldaz A, Feliu JM (2010) CO electrooxidation on carbon supported platinum nanoparticles: effect of aggregation. J Electroanal Chem 644:117–126

Lu G, Ning F, Wei J, Li Y, Bai C, Shen Y, Li Y, Zhou X (2020) All-solid-state passive direct methanol fuel cells with great orientation stability and high energy density based on solid methanol fuels. J Power Sources 450:227669

Łukaszewski M (2016) Electrochemical methods of real surface area determination of noble metal electrodes–an overview. Int J Electrochem Sci 4442–4469.

Maillard F, Savinova ER, Simonov PA, Zaikovskii VI, Stimming U (2004) Infrared spectroscopic study of CO adsorption and electrooxidation on carbon-supported pt nanoparticles: interparticle versus intraparticle heterogeneity. J Phys Chem B 108:17893–17904

Markovic N (2002) Surface science studies of model fuel cell electrocatalysts. Surf Sci Rep 45:117–229

Massong H, Wang H, Samjeské G, Baltruschat H (2001) The co-catalytic effect of Sn, Ru and Mo decorating steps of Pt(111) vicinal electrode surfaces on the oxidation of CO. Electrochim Acta 46:701–707

Masud J, Alam MT, Miah MR, Okajima T, Ohsaka T (2011a) Enhanced electrooxidation of formic acid at Ta2O5-modified Pt electrode. Electrochem Commun 13:86–89

Masud J, Alam MT, Okajima T, Ohsaka T (2011b) Catalytic electrooxidation of formaldehyde at Ta 2 O 5 -modified Pt electrodes. Chem Lett 40:252–254

Masud J, Alam MT, Awaludin Z, El-Deab MS, Okajima T, Ohsaka T (2012) Electrocatalytic oxidation of methanol at tantalum oxide-modified Pt electrodes. J Power Sources 220:399–404

Maya-Cornejo J, Guerra-Balcázar M, Arjona N, Álvarez-Contreras L, Rodríguez Valadez FJ, Gurrola MP, Ledesma-García J, Arriaga LG (2016) Electrooxidation of crude glycerol as waste from biodiesel in a nanofluidic fuel cell using Cu@Pd/C and Cu@Pt/C. Fuel 183:195–205

Mikkelsen K, Cassidy B, Hofstetter N, Bergquist L, Taylor A, Rider DA (2014) Block copolymer templated synthesis of core-shell PtAu bimetallic nanocatalysts for the methanol oxidation reaction. Chem Mater 26:6928–6940

Moura Souza F, Parreira LS, Hammer P, Batista BL, Santos MC (2018) Niobium: a promising Pd co-electrocatalyst for ethanol electrooxidation reactions. J Solid State Electrochem 22:1495–1506

Neto AO, Vasconcelos TRR, Silva RWRVD, LinardiSpinacé MEV (2005) Electro-oxidation of ethylene glycol on PtRu/C and PtSn/C electrocatalysts prepared by alcohol-reduction process. J Appl Electrochem 35:193–198

Oliveira CP, Lussari NV, Sitta E, Varela H (2012) Oscillatory electro-oxidation of glycerol on platinum. Electrochim Acta 85:674–679

Ong BC, Kamarudin SK, Basri S (2017) Direct liquid fuel cells: a review. Int J Hydrogen Energy 42:10142–10157

Ottoni CA, da Silva SG, De Souza RFB, Neto AO (2016) Glycerol oxidation reaction using PdAu/C electrocatalysts. Ionics (kiel) 22:1167–1175

Paganoto GT, Santos DM, Evangelista TCS, Guimarães MCC, Carneiro MTWD, Ribeiro J (2017) Electrochemical and morphological investigations of Ga addition to Pt electrocatalyst supported on carbon. Sci World J 2017:1–15

Palma LM, Almeida TS, Leonello PH, Andrade ARD (2014) Ethanol electrooxidation by plurimetallic Pt-based electrocatalysts prepared by microwave assisted heating. J Electrochem Soc 161:F473–F479

Pan Z, Huang B, An L (2019) Performance of a hybrid direct ethylene glycol fuel cell. Int J Energy Res 43:2583–2591

Papageorgopoulos D, Keijzer M, de Bruijn F (2002) The inclusion of Mo, Nb and Ta in Pt and PtRu carbon supported electrocatalysts in the quest for improved CO tolerant PEMFC anodes. Electrochim Acta 48:197–204

Pedicini R, Schiavo B, Rispoli P, Saccà A, Carbone A, Gatto I, Passalacqua E (2014) Progress in polymeric material for hydrogen storage application in middle conditions. Energy 64:607–614

Planes GA, García G, Pastor E (2007) High performance mesoporous Pt electrode for methanol electrooxidation. A DEMS Study Electrochem Commun 9:839–844

Polonský J, Petrushina IM, Christensen E, Bouzek K, Prag CB, Andersen JET, Bjerrum NJ (2012) Tantalum carbide as a novel support material for anode electrocatalysts in polymer electrolyte membrane water electrolysers. Int J Hydrogen Energy 37:2173–2181

Puthiyapura VK, Lin W-F, Russell AE, Brett DJL, Hardacre C (2018) Effect of mass transport on the electrochemical oxidation of alcohols over electrodeposited film and carbon-supported Pt electrodes. Top Catal 61:240–253

Queiroz MAR, Ribeiro J (2019) Catalysts of PtSn/C modified with Ru and Ta for electrooxidation of ethanol. Catalysts 9:277

Rahsepar M, Pakshir M, Piao Y, Kim H (2012) Synthesis and electrocatalytic performance of high loading active PtRu multiwalled carbon nanotube catalyst for methanol oxidation. Electrochim Acta 71:246–251

Reid O, Saleh FS, Easton EB (2013) Determining electrochemically active surface area in PEM fuel cell electrodes with electrochemical impedance spectroscopy and its application to catalyst durability. Electrochim Acta 114:278–284

Ribeiro J, dos Anjos DM, Kokoh KB, Coutanceau C, Léger J-M, Olivi P, de Andrade AR, Tremiliosi-Filho G (2007) Carbon-supported ternary PtSnIr catalysts for direct ethanol fuel cell. Electrochim Acta 52:6997–7006

Ribeiro J, dos Anjos DM, Léger JM, Hahn F, Olivi P, de Andrade AR, Tremiliosi-Filho G, Kokoh KB (2008) Effect of W on PtSn/C catalysts for ethanol electrooxidation. J Appl Electrochem 38:653–662

Ribeiro J, Tremiliosi-Filho G, Olivi P, de Andrade AR (2011) XAS characterization of the RuO2–Ta2O5 system local (crystal) structure. Mater Chem Phys 125:449–460

Rizo R, Sebastián D, Lázaro MJ, Pastor E (2017) On the design of Pt-Sn efficient catalyst for carbon monoxide and ethanol oxidation in acid and alkaline media. Appl Catal B Environ 200:246–254

Saleh FS, Easton EB (2014) Assessment of the ethanol oxidation activity and durability of Pt catalysts with or without a carbon support using electrochemical impedance spectroscopy. J Power Sources 246:392–401

Santiago EI, Batista MS, Assaf EM, Ticianelli EA (2004) Mechanism of CO tolerance on molybdenum-based electrocatalysts for PEMFC. J Electrochem Soc 151:A944

Santos DM, Paganoto GT, Queiroz MAR, Guimarães MCC and Ribeiro J (2017a) Influence of support material of PtSnNiGa/C electrocatalysts for ethanol oxidation. Orbital–Electron. J Chem 9.

Scibioh MA, Kim S-K, Cho EA, Lim T-H, Hong S-A, Ha HY (2008) Pt-CeO2/C anode catalyst for direct methanol fuel cells. Appl Catal B Environ 84:773–782

Shao-Horn Y, Sheng WC, Chen S, Ferreira PJ, Holby EF, Morgan D (2007) Instability of supported platinum nanoparticles in low-temperature fuel cells. Top Catal 46:285–305

Silva MF, Delmonde MVF, Batista BC, Boscheto E, Varela H, Camara GA (2019) Oscillatory electro-oxidation of ethanol on platinum studied by in situ ATR-SEIRAS. Electrochim Acta 293:166–173

Sitta E, Nascimento MA, Varela H (2010) Complex kinetics, high frequency oscillations and temperature compensation in the electro-oxidation of ethylene glycol on platinum. Phys Chem Phys 12:15195

Soloveichik GL (2014) Liquid fuel cells. Beilstein J Nanotechnol 5:1399–1418

Souza FM, Böhnstedt P, Pinheiro VS, Oliveira LA, Batista BL, Parreira LS, Antunes RA, Santos MC (2020) Niobium increasing the electrocatalytic activity of palladium for alkaline direct ethanol fuel cell. J Electroanal Chem 858:113824

Souza FM, Pinheiro VS, Gentil TC, Batista BL, Parreira LS, Santos MC (2021) NaNbO3 microcubes decorated with minimum Pd and maximum performance for Alkaline direct ethanol fuel cell applications. J Power Sources 493:229694

Spendelow JS, Lu GQ, Kenis PJA, Wieckowski A (2004) Electrooxidation of adsorbed CO on Pt(111) and Pt(111)/Ru in alkaline media and comparison with results from acidic media. J Electroanal Chem 568:215–224

Sudachom N, Warakulwit C, Prapainainar C, Witoon T, Prapainainar P (2017) One step NaBH4 reduction of Pt-Ru-Ni catalysts on different types of carbon supports for direct ethanol fuel cells: synthesis and characterization. J Fuel Chem Technol 45:596–607

Tayal J, Rawat B, Basu S (2011) Bi-metallic and tri-metallic Pt–Sn/C, Pt–Ir/C, Pt–Ir–Sn/C catalysts for electro-oxidation of ethanol in direct ethanol fuel cell. Int J Hydrogen Energy 36:14884–14897

Teran FE, Santos DM, Ribeiro J, Kokoh KB (2012) Activity of PtSnRh/C nanoparticles for the electrooxidation of C1 and C2 alcohols. Thin Solid Films 520:5846–5850

Ueda A, Yamada Y, Ioroi T, Fujiwara N, Yasuda K, Miyazaki Y, Kobayashi T (2003) Electrochemical oxidation of CO in sulfuric acid solution over Pt and PtRu catalysts modified with TaOx and NbOx. Catal Today 84:223–229

Verma M, Sinha L, Shirage PM (2021) Electrodeposited nanostructured flakes of cobalt, manganese and nickel-based sulfide (CoMnNiS)

for electrocatalytic alkaline oxygen evolution reaction (OER). J Mater Sci Mater Electron 32:12292–12307

Wang H, Löffler T, Baltruschat H (2001) Formation of intermediates during methanol oxidation: a quantitative DEMS study. J Appl Electrochem 31:759–765

Wiltshire RJK, King CR, Rose A, Wells PP, Davies H, Hogarth MP, Thompsett D, Theobald B, Mosselmans FW, Roberts M, Russell AE (2009) Effects of composition on structure and activity of PtRu/C catalysts. Phys Chem Phys 11:2305

Wu HW (2016) A review of recent development: transport and performance modeling of PEM fuel cells. Appl Energy 165:81–106

Xin Y, Shen PK (2017) Tantalum carbide doped by fluorine as nonprecious metal anodic electrocatalyst superior to Pt/C for glycerol-oxidation. Electrochim Acta 227:267–274

Zana A, Speder J, Roefzaad M, Altmann L, Bäumer M, Arenz M (2013) Probing degradation by IL-TEM: the influence of stress test conditions on the degradation mechanism. J Electrochem Soc 160:F608–F615

Zhang X, Li H, Yang J, Lei Y, Wang C, Wang J, Tang Y, Mao Z (2021) Recent advances in Pt-based electrocatalysts for PEMFCs. RSC Adv 11:13316–13328

Zhao Y, Wu L, Zhou K, Lang J, Wang G, Tian P, Wang X (2019) Palladium-loaded tantalum oxide modified Pt electrode toward electrochemical oxidation of ethylene glycol. J Electroanal Chem 839:166–172

Zheng L, Xiong L, Liu Q, Han K, Liu W, Li Y, Tao K, Niu L, Yang S, Xia J (2011) Enhanced electrocatalytic activity for the oxidation of liquid fuels on PtSn nanoparticles. Electrochim Acta 56:9860–9867